

Superradiant scattering by rotating black-bounce black holes

Pedro Henrique Croti Siqueira^{1, 2, *} and Maurício Richartz^{1, †}

¹*Centro de Matemática, Computação e Cognição,*

Universidade Federal do ABC (UFABC), 09210-170 Santo André, São Paulo, Brazil

²*Centro de Ciências Naturais e Humanas, Universidade Federal do ABC (UFABC), 09210-170 Santo André, São Paulo, Brazil*

We investigate superradiant scattering off a rotating regular black hole described by a black-bounce metric which generalizes the Kerr spacetime of mass M and specific angular momentum a through a regularization parameter p and two deformation exponents (k, n) . Focusing on massless $(\ell, m) = (1, 1)$ scalar modes, we explore the parameter space and compute amplification factors by numerically integrating the separated radial Klein–Gordon equation. We track the peak amplification and the corresponding frequency across the $(a/M, p/M)$ parameter space for several combinations of k and n . We find that increasing n systematically enhances superradiance, whereas increasing k tends to suppress it. In particular, certain configurations yield amplification levels up to 98% larger than the maximum amplification for standard Kerr black holes.

I. INTRODUCTION

The detection of gravitational waves by observatories such as LIGO, Virgo, and KAGRA has opened new perspectives for testing the strong field regime of gravity [1–6]. In this context, the so-called Kerr hypothesis, which posits that astrophysical black holes are accurately described by the Kerr metric, has been extensively scrutinized [7, 8]. Although current observations are largely consistent with this paradigm, uncertainties in the inferred masses and spins of compact objects leave room for deviations from the Kerr geometry and for alternative theories of gravity [9–13], thus motivating the investigation of more general, possibly regular, black hole solutions [14].

Regular black holes possess an event horizon while remaining free from curvature singularities [15, 16]. The existence of regular black holes inevitably requires a violation of the strong energy condition in general relativity [17, 18]. The first example of such an object was introduced by Bardeen [19] and, since then, a variety of regular geometries have been idealized within classical or semiclassical frameworks [20–31]. Among the most recent proposals is the black-bounce spacetime introduced by Simpson and Visser [17, 32, 33], which describes either a regular black hole or a traversable wormhole depending on the values of the parameters that define the metric. In recent years, numerous studies have explored the structure of black-bounce spacetimes and their properties [17, 34–52].

Although the original Simpson-Visser spacetime is static, subsequent rotating generalizations have also attracted significant attention [53–64]. These geometries extend the classical Kerr solution by incorporating a regular core, while retaining key features such as an ergoregion. In particular, rotating regular black holes can sup-

port wave scattering phenomena similar to those found in the Kerr spacetime. Among these phenomena, superradiance stands out as a particularly remarkable effect in which low-frequency waves interacting with the rotating geometry can be amplified [65–67]. Superradiant amplification typically occurs when the wave frequency ω and the azimuthal number m satisfy

$$0 < \omega < m\Omega_H, \quad (1.1)$$

where Ω_H is the angular velocity of the event horizon. The process extracts rotational energy from the black hole and may lead to instabilities when the field is massive [68–71].

In the present work, we explore the occurrence of superradiance in the rotating black-bounce geometry introduced in Ref. [54], which generalizes the black-bounce geometries of Refs. [32, 53]. By analyzing the scattering of massless scalar fields, we investigate how the deformation parameters of the metric affect the efficiency of superradiant amplification, specially in the large spin regime. In particular, our goal is to determine the peak amplification (and the associated frequency) in several deformation scenarios and to compare it against the maximum amplification achieved for Kerr black holes.

This work is organized as follows. In Sec. II, we introduce the Kerr-like black-bounce metric, discuss the associated spacetime structure, and examine the Klein–Gordon equation that governs the propagation of scalar fields. In Sec. III, we outline the numerical scheme employed to solve the wave equation and explore the dependence of the superradiant amplification factor on the parameters that characterize deviations from the Kerr geometry. Finally, Sec. IV is dedicated to our concluding remarks. Throughout this work we use $G = c = \hbar = 1$ units.

II. KERR-LIKE BLACK-BOUNCE SPACETIMES

We consider the rotating regular black hole geometry obtained in Ref. [54] by applying the Newman-Janis

* pedro.croti@ufabc.edu.br

† mauricio.richartz@ufabc.edu.br

algorithm to a static black-bounce metric. The spacetime, which generalizes the rotating Simpson-Visser solution [32, 53], is characterized by the line element

$$ds^2 = - \left[1 - \frac{2M(r^2 + p^2)r^k}{(r^{2n} + p^{2n})^{\frac{k+1}{2n}} \Sigma} \right] dt^2 + \frac{\Sigma}{\Delta} dr^2 + \Sigma d\theta^2 - \frac{4a \sin^2 \theta}{\Sigma} \frac{M(r^2 + p^2)r^k}{(r^{2n} + p^{2n})^{\frac{k+1}{2n}}} dt d\phi + \frac{\sin^2 \theta}{\Sigma} [(r^2 + p^2 + a^2)^2 - a^2 \Delta \sin^2 \theta] d\phi^2, \quad (2.1)$$

with

$$\Delta = r^2 + p^2 + a^2 - \frac{2M(r^2 + p^2)r^k}{(r^{2n} + p^{2n})^{\frac{k+1}{2n}}}, \quad (2.2)$$

$$\Sigma = r^2 + p^2 + a^2 \cos^2 \theta. \quad (2.3)$$

Here, M is the mass of the spacetime, a is the specific angular momentum, and p is the black-bounce regularization parameter. The integers $k \geq 0$ and $n \geq 1$ are referred to as the deformation parameters. The choice $(k, n) = (0, 1)$ yields the rotating Simpson-Visser spacetime, while $(k, n) = (2, 1)$ corresponds to the rotating Bardeen-like spacetime [17, 54]. Note that, regardless of the deformation exponents k and n , the spacetime reduces to the Kerr spacetime when $p = 0$. In contrast, a nonvanishing parameter p removes the central singularity and, together with (k, n) , controls the deviation from Kerr. In particular, the spacetime corresponds to a traversable wormhole when $p > p_c$ and to a regular black hole when $0 < p < p_c$, where the critical black-bounce parameter p_c depends on the spin as well as on the deformation exponents [54].

In Fig. 1, we show the location r_0 of the event horizon for black holes described by the metric (2.1). Each panel, corresponding to a particular choice of the pair (k, n) , exhibits the dependence of r_0/M on both the dimensionless spin a/M and the black-bounce parameter p/M . The white region in each panel corresponds to wormhole configurations (when $p > 0$) and to naked singularities (when $p = 0$). The green colored regions correspond to black hole configurations.

We observe a clear distinction between the $n = 1$ and the $n > 1$ families. For $n = 1$, the horizon radius r_0/M decreases monotonically with increasing a/M and p/M , for all values of k . Moreover, for fixed $(a/M, p/M)$, larger k values lead to smaller black holes. For $n > 1$, the dependence on spin is analogous: r_0/M decreases with a/M . However, the dependence on the black-bounce parameter p/M becomes non-monotonic. In particular, for each fixed k , the horizon radius initially increases with p/M , reaches a maximum at an intermediate value, and then decreases for larger p/M .

Regarding the role of the parameters (k, n) , we note that while $n = 1$ does not admit ultra-spinning (i.e., $a/M > 1$) black hole configurations, the $n > 1$ family does, as shown in the second and third columns of Fig. 1.

In particular, for the $n = 2$ and $n = 3$ configurations, the allowed range of black hole spins increases with p/M , up to a critical value at which the maximum admissible spin is reached. We also observe that, for fixed n , larger values of k progressively restrict the black hole parameter space.

A. Scalar field dynamics

We are interested in the dynamics of a test massless scalar field Φ propagating in rotating regular black-bounce geometries described by (2.1). The scalar field obeys the Klein-Gordon equation

$$\frac{1}{\sqrt{-g}} \partial_\mu (g^{\mu\nu} \sqrt{-g} \partial_\nu \Phi) = 0, \quad (2.4)$$

which can be separated due to the symmetries of the spacetime. In fact, given the stationarity and axisymmetry of the background, we decompose the scalar field into modes of frequency ω , azimuthal number $m \in \mathbb{Z}$, and orbital number $\ell \geq m$ using the standard ansatz

$$\Phi_{\omega\ell m}(t, \phi, \theta, r) = e^{-i\omega t + im\phi} R_{\omega\ell m}(r) S_{\omega\ell m}(\theta). \quad (2.5)$$

This decomposition leads to decoupled radial and angular equations, involving a separation constant $\lambda_{\omega\ell m}$. The angular part yields spheroidal harmonics satisfying

$$\frac{1}{\sin \theta} \frac{d}{d\theta} \left(\sin \theta \frac{dS_{\omega\ell m}}{d\theta} \right) + \left(\lambda_{\omega\ell m} - a^2 \omega^2 \cos^2 \theta - \frac{m^2}{\sin^2 \theta} \right) S_{\omega\ell m} = 0. \quad (2.6)$$

The radial equation, on the other hand, takes the form

$$\Delta \frac{d}{dr} \left(\Delta \frac{dR_{\omega\ell m}}{dr} \right) + \left[(-\omega(r^2 + p^2 + a^2) + am)^2 - \lambda_{\omega\ell m} \Delta \right] R_{\omega\ell m} = 0. \quad (2.7)$$

For simplicity, we shall omit the indices $\omega\ell m$ in $R_{\omega\ell m}$, $S_{\omega\ell m}$, and $\lambda_{\omega\ell m}$.

The solution of the radial equation which corresponds to ingoing waves in the near-horizon regime ($r \rightarrow r_0$) is given by

$$R(r) \approx (r - r_0)^{-\frac{i(a^2 + p^2 + r_0^2)}{\Delta'(r_0)}(\omega - m\Omega_H)}, \quad (2.8)$$

with primes denoting derivatives with respect to r and

$$\Omega_H = \frac{a}{a^2 + p^2 + r_0^2}. \quad (2.9)$$

In contrast, at spatial infinity, the asymptotic solution is given by

$$R(r) \approx \mathcal{I} e^{-i\omega r} r^{-1-2iM\omega} + \mathcal{R} e^{i\omega r} r^{-1+2iM\omega}, \quad (2.10)$$

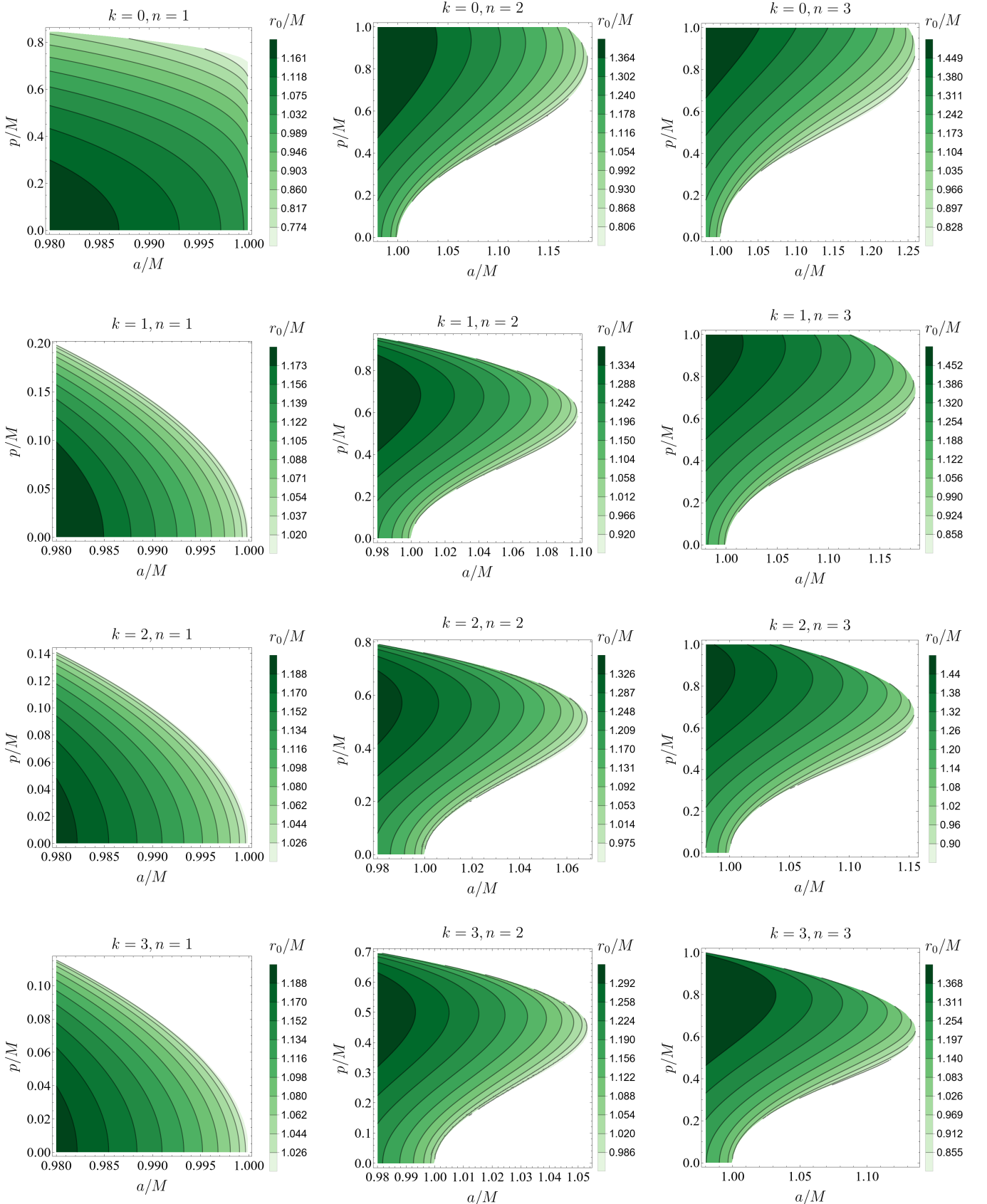


FIG. 1. Contour plots of the event horizon radius r_0/M as a function of the parameters a/M and p/M for different values of the deformation exponents k and n . Each column corresponds to a given $n \in \{1, 2, 3\}$, while each row corresponds to a given $k \in \{0, 1, 2, 3\}$. The panels highlight how the interplay between spin, black-bounce parameter and deformation exponents constrains the parameter space of black hole configurations.

where \mathcal{I} and \mathcal{R} are related to the amplitudes of the incident and reflected waves, respectively. The superradiant amplification factor Z is defined as

$$Z = Z(M\omega, p/M, a/M, k, n, \ell, m) = \frac{|\mathcal{R}|^2}{|\mathcal{I}|^2} - 1. \quad (2.11)$$

III. AMPLIFICATION FACTORS

A. Numerical scheme

To compute the amplification factor Z , we solve the scattering problem using the following numerical procedure. For fixed deformation exponents (k, n) , and for each choice of spin a/M and black-bounce parameter p/M , we first determine the roots of the metric function $\Delta(r)$ and identify the position r_0 of the event horizon. We then fix the mode parameters (ℓ, m) and the frequency ω , and solve the radial wave equation (2.7) by imposing initial conditions near the event horizon, specifically at $r_1 = r_0 + 10^{-8}$. The radial equation is integrated numerically up to $r_2 = 200M$, where we extract the radial function R and its derivative. Using $R(r_2)$ and $R'(r_2)$, we compute the incident and reflected parameters, respectively \mathcal{I} and \mathcal{R} , via (2.10), and hence obtain the amplification factor Z from Eq. (2.11). Keeping all other parameters fixed, we then vary ω and repeat the numerical integration to determine the maximum amplification with respect to the frequency,

$$\bar{Z} = \max\{Z : M\omega \in \mathbb{R}\}, \quad (3.1)$$

together with the corresponding frequency $\bar{\omega}$.

To investigate the impact of deviations from the Kerr geometry on superradiance, we compute \bar{Z} and $\bar{\omega}$ as we scan the parameter space $(a/M, p/M)$. We focus on $(\ell, m) = (1, 1)$ modes in the high spin regime, where superradiant amplification is strongest for Kerr black holes. The scan starts at $a/M = 0.98$ and $p/M = 0$, corresponding to a rapidly rotating Kerr black hole, for which the peak amplification is expected to occur at $M\omega \sim 0.38$ [72]. From this initial point, we increase the spin a/M in steps $\Delta a/M$ and, at each step, verify whether an event horizon still exists. Whenever it does, we compute a new set of amplification factors Z using a refined frequency interval centered on the peak amplification of the previous iteration:

$$M\omega \in [M\bar{\omega}_i - 0.03, M\bar{\omega}_i + 0.03], \quad (3.2)$$

where $M\bar{\omega}_i$ denotes the peak frequency obtained for the preceding spin value. From this dataset, we extract the peak amplification \bar{Z} and the corresponding frequency $\bar{\omega}$ at the current spin. For each fixed a/M , we then perform a scan in the p -direction, increasing the black-bounce parameter from $p/M = 0$ up to $p/M = 1$ in steps of $\Delta p/M$. Using an analogous refinement procedure, we

determine \bar{Z} and $\bar{\omega}$ for each pair $(a/M, p/M)$ in the parameter space. The increments $\Delta a/M$ and $\Delta p/M$ are chosen to ensure adequate resolution in the resulting figures.

Once the full $(a/M, p/M)$ domain of interest has been scanned, we identify the maximum superradiant amplification factor \bar{Z}_{\max} across the parameter space for the chosen pairs (ℓ, m) and (k, n) ,

$$\bar{Z}_{\max} = \max\{\bar{Z} : a/M \geq 0.98, p/M \geq 0\}. \quad (3.3)$$

We denote the corresponding frequency by $\bar{\omega}_{\max}$, and the location in parameter space where this maximum is attained by $(a_{\max}/M, p_{\max}/M)$. To improve the precision of our analysis, we perform a secondary, high-resolution scan in a narrower region around this point,

$$a/M \in [a_{\max}/M - 0.001, a_{\max}/M + 0.001], \quad (3.4)$$

$$p/M \in [p_{\max}/M - 0.005, p_{\max}/M + 0.005], \quad (3.5)$$

using smaller steps $\Delta a/M = 0.0001$ and $\Delta p/M = 0.0001$. This high-resolution scan is then used to refine the values of \bar{Z}_{\max} , $M\bar{\omega}_{\max}$, a_{\max}/M , and p_{\max}/M .

B. Numerical results

Our main results are presented in Figs. 2 and 3. We consider twelve representative cases: all combinations (k, n) satisfying $0 \leq k \leq 3$ and $1 \leq n \leq 3$. Fig. 2 displays the maximum amplification factor \bar{Z} at each point $(a/M, p/M)$, normalized to the Kerr global maximum $\bar{Z}_{\max}^{\text{Kerr}} \simeq 0.003674$, which occurs at $a/M \approx 0.9872$ [72]. Fig. 3 shows the frequency $M\bar{\omega}$ associated with the peak amplification at each point in parameter space. In both figures, the red dot marks the location $(a_{\max}/M, p_{\max}/M)$ where the maximum amplification within each panel, i.e. \bar{Z}_{\max} , is attained. As seen in Fig. 3, the frequency $\bar{\omega}_{\max}$ corresponding to \bar{Z}_{\max} in each panel does not coincide with the global maximum of $\bar{\omega}$.

The first column of Figs. 2 and 3 corresponds to the case $n = 1$, namely the configurations $(k, n) = (0, 1)$, $(1, 1)$, $(2, 1)$, and $(3, 1)$. From Fig. 2 we observe that, for $n = 1$, the peak amplification \bar{Z} decreases monotonically with increasing p/M at fixed a/M . Conversely, for sufficiently small values of p/M , the dependence of the peak amplification on the spin is nonmonotonic: \bar{Z} initially increases with a/M , reaches a local maximum, and then decreases as $a/M \rightarrow 1$. In particular, we verify that superradiance is maximized at $p/M = 0$ and $a/M = 0.9872$, which coincides with the spin value that maximizes superradiance in the Kerr spacetime. As a consequence, for $n = 1$, the superradiant amplification of regular rotating black-bounce spacetimes never exceeds the Kerr maximum. In other words, the largest amplification is always achieved in the Kerr limit, and the black-bounce deformation does not enhance superradiance. The corresponding peak frequencies are shown in the first column

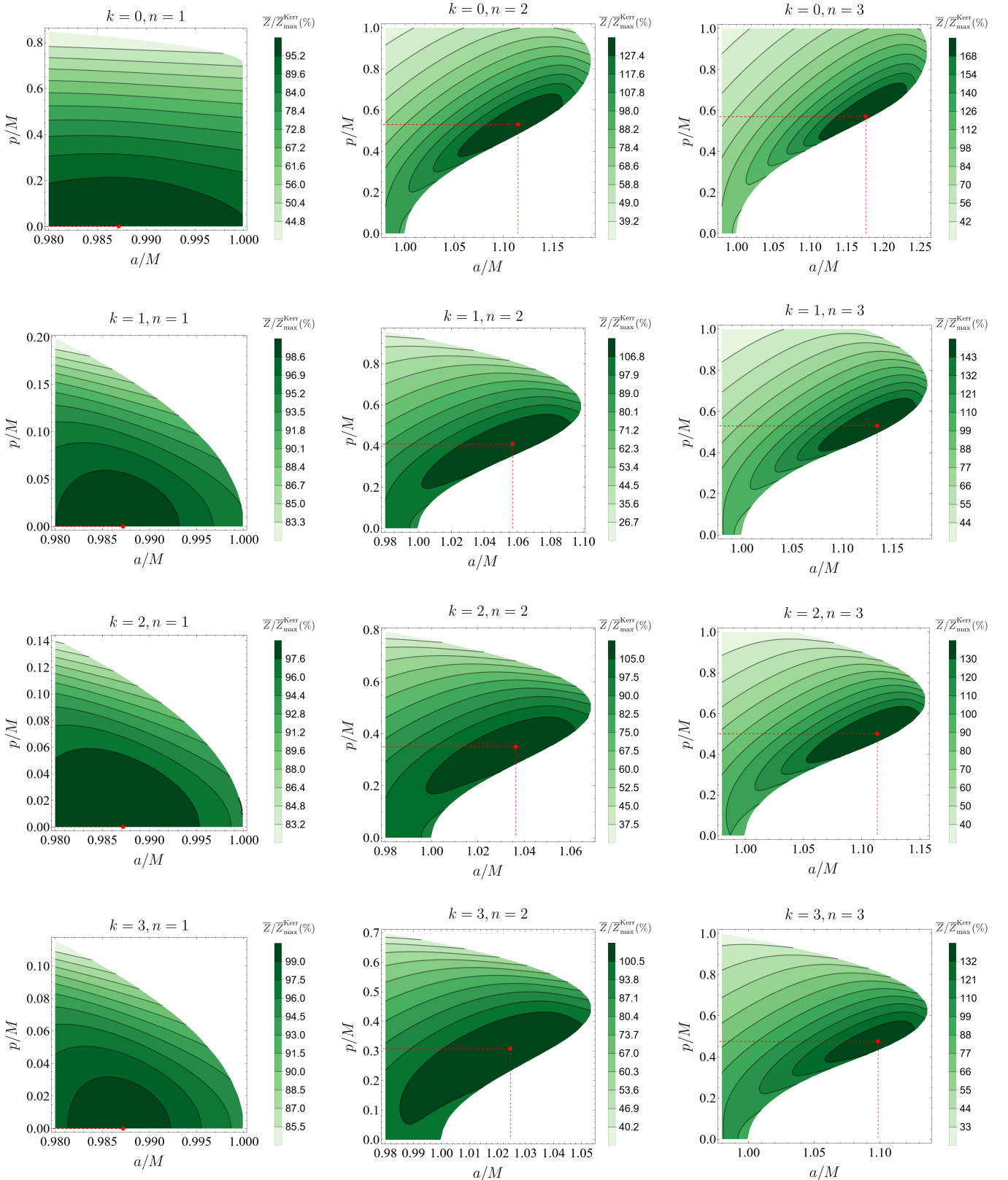


FIG. 2. Contour plots of the relative maximum superradiant amplification $\bar{Z}/\bar{Z}_{\max}^{\text{Kerr}}$ in the $(a/M, p/M)$ parameter space for different values of the deformation exponents k and n . Each column corresponds to a fixed $n = 1, 2, 3$, and each row to a fixed $k = 0, 1, 2, 3$. The color scale quantifies the enhancement or suppression of the amplification relative to the Kerr case, highlighting how deviations controlled by p/M and the deformation exponents modify the efficiency of superradiant scattering. The red dot in each panel denotes the location of the global maximum \bar{Z}_{\max} .

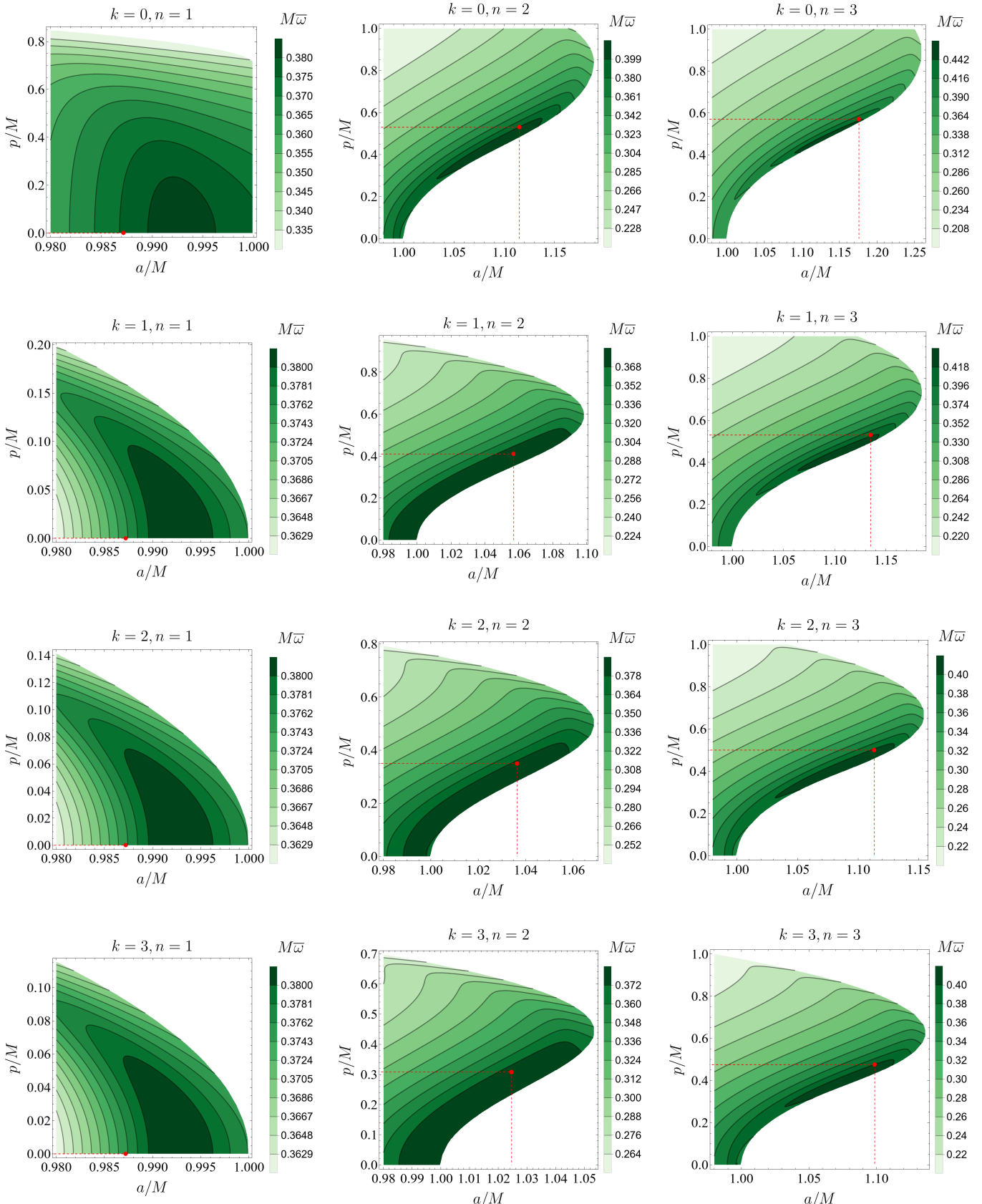


FIG. 3. Contour plots of the frequency $M\bar{\omega}$ associated with the maximum superradiant amplification in the $(a/M, p/M)$ parameter space for different values of the deformation exponents k and n . Each column corresponds to a fixed $n = 1, 2, 3$, and each row to a fixed $k = 0, 1, 2, 3$. The color scale indicates the value of $M\bar{\omega}$, illustrating how the peak frequency shifts with the spin a/M , the black-bounce parameter p/M , and the deformation exponents. The red dot in each panel marks the location of the global maximum \bar{Z}_{\max} shown in Fig. 2.

of Fig. 3. For sufficiently small p/M , the peak frequency exhibits a nonmonotonic dependence on the spin, increasing with a/M before decreasing as the extremal limit is approached.

Next, we examine $n > 1$ configurations, specifically $n = 2$ and $n = 3$, which allow for superspinning $a/M > 1$ black holes. The results are presented in the second and third columns of Figs. 2 and 3. In contrast to the $n = 1$ case, we find regions of the parameter space $(a/M, p/M)$ where the superradiant amplification exceeds the maximum amplification for Kerr black holes. Table I shows the parameter values corresponding to the global maxima of superradiance in each of the $n > 1$ configurations. For instance, when $(k, n) = (0, 3)$, we find that the amplification factor can be as high as 198% of the Kerr result, indicating that black-bounce deformations can significantly enhance superradiant effects.

| (k, n) | a_{\max}/M | p_{\max}/M | $M\bar{\omega}_{\max}$ | \bar{Z}_{\max} | $\bar{Z}_{\max}/\bar{Z}_{\max}^{\text{Kerr}}$ |
|----------|--------------|--------------|------------------------|------------------|---|
| (0,2) | 1.115 | 0.53 | 0.4003 | 0.005236 | 142% |
| (1,2) | 1.057 | 0.41 | 0.3868 | 0.004425 | 120% |
| (2,2) | 1.036 | 0.35 | 0.3830 | 0.004173 | 114% |
| (3,2) | 1.025 | 0.31 | 0.3810 | 0.004048 | 110% |
| (0,3) | 1.176 | 0.57 | 0.4351 | 0.007273 | 198% |
| (1,3) | 1.135 | 0.53 | 0.4130 | 0.006037 | 164% |
| (2,3) | 1.113 | 0.50 | 0.4049 | 0.005553 | 151% |
| (3,3) | 1.099 | 0.47 | 0.4011 | 0.005279 | 144% |

TABLE I. Global maxima of the superradiant amplification factor for deformation exponents $n = 2$ and $n = 3$, with $0 \leq k \leq 3$. For each configuration, we list the maximum amplification factor \bar{Z}_{\max} and its ratio relative to the Kerr value $\bar{Z}_{\max}^{\text{Kerr}}$, together with the corresponding values of the spin parameter a_{\max}/M , the black-bounce parameter p_{\max}/M , and the frequency $M\bar{\omega}_{\max}$ at which the maximum occurs.

To isolate the effects of the deformation exponents k and n , we consider variations at fixed n and at fixed k . Examining a given row of Fig. 2 allows us to assess the effect of increasing n for fixed values of $k = 0, 1, 2$, and 3. We find that increasing n not only shifts the location of the amplification peak in parameter space towards larger a/M and p/M , but also leads to an enhancement of the superradiant amplification relative to the Kerr case. Conversely, examining a fixed column of Fig. 2 highlights the effect of increasing k for fixed $n = 1, 2$, and 3. For $n = 1$, increasing k from 0 to 3 produces no change in the maximum amplification, since the superradiant peak always coincides with the Kerr limit. For $n = 2$ and $n = 3$, increasing k tends to suppress the strength of superradiance. Table I shows that increasing k from 0 to 3 reduces the enhancement of superradiance from 142% to 110% when $n = 2$. Similarly, for $n = 3$, the enhancement is reduced from 198% at $k = 0$ to 144% at $k = 3$.

IV. FINAL REMARKS

In this work, we investigated the superradiant scattering of massless scalar fields by a rotating black-bounce spacetime, a regular geometry that extends the Simpson–Visser solution through a set of deformation parameters. By varying the pair (k, n) characterizing the metric, together with the black-bounce parameter p/M and the dimensionless spin a/M , we mapped the behavior of the superradiant amplification factor over a broad region of the parameter space. Our results show that certain combinations of parameters lead to substantial deviations from the Kerr black hole scenario. In particular, we identified regimes, specifically for $n > 1$, in which the superradiant amplification exceeds the Kerr maximum by up to 98%. These enhancements appear to be associated with modifications of the near-horizon geometry induced by the regularity structure which allow for superspinning configurations with $a/M > 1$.

An important outcome of our analysis is the identification of a nontrivial dependence of the peak amplification on the black-bounce parameter p/M . In several cases, the amplification exhibits a nonmonotonic behavior as p/M increases, indicating the existence of optimal configurations for energy extraction. We were also able to investigate the roles of the deformation exponents k and n . We find that the parameter n plays a central role in enabling ultra-spinning configurations as p/M increases, with larger n leading to enhanced superradiant amplification. In contrast, increasing k tends to suppress superradiance.

Although our focus has been restricted to massless scalar fields, which provide a useful toy model for probing aspects of gravitational-wave physics, the analysis developed here opens avenues for future investigation. Natural extensions include the study of electromagnetic and gravitational perturbations, as well as stability analyses in the ultra-spinning regime. One can also ask whether the enhancement of superradiance persists in the presence of massive scalar fields, a situation in which superradiant scattering is typically accompanied by quasibound states and instabilities [69, 71, 73–75]. Such instabilities may arise spontaneously in astrophysical environments, particularly when the compact object is surrounded by a massive bosonic field [75, 76], potentially leading to the formation of long-lived bosonic clouds that emit nearly monochromatic gravitational waves. The detection of such signals would provide indirect evidence for ultra-light bosons and place constraints on their masses [77]. A detailed analysis of the spectrum and lifetimes of these states could therefore shed light on the formation of bosonic clouds around regular rotating geometries, constrain the parameter space of black-bounce spacetimes, and assess their viability as beyond-Kerr alternatives in the era of multi-messenger astronomy. Finally, the role of exceptional points and their associated phenomenology, an area that has attracted significant attention recently [78–83], constitutes another promising direction

for future work.

DATA AVAILABILITY

Data supporting the findings of this work are openly available [84].

ACKNOWLEDGMENTS

This research was partially financed by the Coordenação de Aperfeiçoamento de Pessoal de Nível Superior (CAPES, Brazil) - Finance Code 001. PHCS acknowledges support from the São Paulo Research Foundation (FAPESP, Brazil), grant 2022/07298-4. MR acknowledges partial support from the Conselho Nacional de Desenvolvimento Científico e Tecnológico (CNPq, Brazil, grant 315991/2023-2), and from the São Paulo Research Foundation (FAPESP, Brazil, grant 2022/08335-0). PHCS thanks the Strong Group at the Niels Bohr Institute for their kind hospitality while part of this work was carried out. The Tycho supercomputer hosted at the SCIENCE HPC center at the University of Copenhagen was used for supporting this work.

[1] O. Dreyer, B. J. Kelly, B. Krishnan, L. S. Finn, D. Garrison, and R. Lopez-Aleman, Black hole spectroscopy: Testing general relativity through gravitational wave observations, *Class. Quant. Grav.* **21**, 787 (2004), arXiv:gr-qc/0309007.

[2] E. Berti, V. Cardoso, and C. M. Will, On gravitational-wave spectroscopy of massive black holes with the space interferometer LISA, *Phys. Rev. D* **73**, 064030 (2006), arXiv:gr-qc/0512160.

[3] E. Berti, J. Cardoso, V. Cardoso, and M. Cavaglia, Matched-filtering and parameter estimation of ring-down waveforms, *Phys. Rev. D* **76**, 104044 (2007), arXiv:0707.1202 [gr-qc].

[4] E. Berti, A. Sesana, E. Barausse, V. Cardoso, and K. Belczynski, Spectroscopy of Kerr black holes with Earth- and space-based interferometers, *Phys. Rev. Lett.* **117**, 101102 (2016), arXiv:1605.09286 [gr-qc].

[5] R. Brito, A. Buonanno, and V. Raymond, Black-hole Spectroscopy by Making Full Use of Gravitational-Wave Modeling, *Phys. Rev. D* **98**, 084038 (2018), arXiv:1805.00293 [gr-qc].

[6] I. Ota and C. Chirenti, Overtones or higher harmonics? Prospects for testing the no-hair theorem with gravitational wave detections, *Phys. Rev. D* **101**, 104005 (2020), arXiv:1911.00440 [gr-qc].

[7] C. Bambi, Testing the Kerr black hole hypothesis, *Mod. Phys. Lett. A* **26**, 2453 (2011), arXiv:1109.4256 [gr-qc].

[8] C. A. R. Herdeiro, Black Holes: On the Universality of the Kerr Hypothesis, *Lect. Notes Phys.* **1017**, 315 (2023), arXiv:2204.05640 [gr-qc].

[9] R. Konoplya and A. Zhidenko, Detection of gravitational waves from black holes: Is there a window for alternative theories?, *Phys. Lett. B* **756**, 350 (2016), arXiv:1602.04738 [gr-qc].

[10] R. M. Santos, R. C. Nunes, and J. C. N. de Araujo, Testing beyond-Kerr spacetimes with GWTC-3, *Eur. Phys. J. C* **84**, 302 (2024), arXiv:2403.17718 [gr-qc].

[11] A. G. Abac *et al.* (LIGO Scientific, Virgo, KAGRA), GW250114: Testing Hawking's Area Law and the Kerr Nature of Black Holes, *Phys. Rev. Lett.* **135**, 111403 (2025), arXiv:2509.08054 [gr-qc].

[12] H. Siegel, N. M. Khusid, M. Isi, and W. M. Farr, GW231123 ringdown: interpretation as multimodal Kerr signal, (2025), arXiv:2511.02691 [gr-qc].

[13] Z. Zhao, S. Shashank, D. Das, and C. Bambi, Testing black hole metrics with binary black hole inspirals, (2025), arXiv:2510.04703 [gr-qc].

[14] R. Carballo-Rubio *et al.*, Towards a non-singular paradigm of black hole physics, *JCAP* **05**, 003, arXiv:2501.05505 [gr-qc].

[15] R. Carballo-Rubio, F. Di Filippo, S. Liberati, and M. Visser, Opening the Pandora's box at the core of black holes, *Class. Quant. Grav.* **37**, 14 (2020), arXiv:1908.03261 [gr-qc].

[16] R. Carballo-Rubio, F. Di Filippo, S. Liberati, and M. Visser, Geodesically complete black holes, *Phys. Rev. D* **101**, 084047 (2020), arXiv:1911.11200 [gr-qc].

[17] F. S. N. Lobo, M. E. Rodrigues, M. V. de Sousa Silva, A. Simpson, and M. Visser, Novel black-bounce spacetimes: wormholes, regularity, energy conditions, and causal structure, *Phys. Rev. D* **103**, 084052 (2021), arXiv:2009.12057 [gr-qc].

[18] O. B. Zaslavskii, Regular black holes and energy conditions, *Phys. Lett. B* **688**, 278 (2010), arXiv:1004.2362 [gr-qc].

[19] J. M. Bardeen, Proceedings of the international conference gr5 (1968).

[20] S. A. Hayward, Formation and evaporation of nonsingular black holes, *Phys. Rev. Lett.* **96**, 031103 (2006).

[21] T. A. Roman and P. G. Bergmann, Stellar collapse without singularities?, *Phys. Rev. D* **28**, 1265 (1983).

[22] I. Dymnikova, Vacuum nonsingular black hole, *General Relativity and Gravitation* **24**, 235 (1992).

[23] Z.-Y. Fan and X. Wang, Construction of Regular Black Holes in General Relativity, *Phys. Rev. D* **94**, 124027 (2016), arXiv:1610.02636 [gr-qc].

[24] S. G. Ghosh, A nonsingular rotating black hole, *Eur. Phys. J. C* **75**, 532 (2015), arXiv:1408.5668 [gr-qc].

[25] S. Ansoldi, Spherical black holes with regular center: A Review of existing models including a recent realization with Gaussian sources, in *Conference on Black Holes and Naked Singularities* (2008) arXiv:0802.0330 [gr-qc].

[26] K. A. Bronnikov and J. C. Fabris, Regular phantom black holes, *Phys. Rev. Lett.* **96**, 251101 (2006), arXiv:gr-qc/0511109.

[27] K. A. Bronnikov, V. N. Melnikov, and H. Dehnen, Regular black holes and black universes, *Gen. Rel. Grav.* **39**, 973 (2007), arXiv:gr-qc/0611022.

[28] N. Uchikata, S. Yoshida, and T. Futamase, New solutions of charged regular black holes and their stability, *Phys. Rev. D* **86**, 084025 (2012), arXiv:1209.3567 [gr-qc].

[29] L. Balart and E. C. Vagenas, Regular black hole metrics and the weak energy condition, *Phys. Lett. B* **730**, 14 (2014), arXiv:1401.2136 [gr-qc].

[30] L. Balart and E. C. Vagenas, Regular black holes with a nonlinear electrodynamics source, *Phys. Rev. D* **90**, 124045 (2014), arXiv:1408.0306 [gr-qc].

[31] H. Culetu, Nonsingular black hole with a nonlinear electric source, *Int. J. Mod. Phys. D* **24**, 1542001 (2015).

[32] A. Simpson and M. Visser, Black-bounce to traversable wormhole, *Journal of Cosmology and Astroparticle Physics* **2019** (02), 042.

[33] A. Simpson, P. Martin-Moruno, and M. Visser, Vaidya spacetimes, black-bounces, and traversable wormholes, *Class. Quant. Grav.* **36**, 145007 (2019), arXiv:1902.04232 [gr-qc].

[34] M. E. Rodrigues and M. V. d. S. Silva, Source of black bounces in general relativity, *Phys. Rev. D* **107**, 044064 (2023), arXiv:2302.10772 [gr-qc].

[35] P. Cañate, Black bounces as magnetically charged phantom regular black holes in Einstein-nonlinear electrodynamics gravity coupled to a self-interacting scalar field, *Phys. Rev. D* **106**, 024031 (2022), arXiv:2202.02303 [gr-qc].

[36] M. E. Rodrigues and M. V. d. S. Silva, Embedding regular black holes and black bounces in a cloud of strings, *Phys. Rev. D* **106**, 084016 (2022), arXiv:2210.05383 [gr-qc].

[37] H. Huang and J. Yang, Charged Ellis Wormhole and Black Bounce, *Phys. Rev. D* **100**, 124063 (2019), arXiv:1909.04603 [gr-qc].

[38] K. A. Bronnikov, M. E. Rodrigues, and M. V. de S. Silva, Cylindrical black bounces and their field sources, *Phys. Rev. D* **108**, 024065 (2023), arXiv:2305.19296 [gr-qc].

[39] M. E. Rodrigues and M. V. d. S. Silva, Spherically symmetric and static black bounces with multiple horizons, throats, and anti-throats in four dimensions, *Class. Quant. Grav.* **42**, 055005 (2025), arXiv:2502.00502 [gr-qc].

[40] G. Alencar, K. A. Bronnikov, M. E. Rodrigues, D. Sáez-Chillón Gómez, and M. V. de S. Silva, On black bounce space-times in non-linear electrodynamics, *Eur. Phys. J. C* **84**, 745 (2024), arXiv:2403.12897 [gr-qc].

[41] C. F. S. Pereira, M. V. d. S. Silva, H. Belich, D. C. Rodrigues, J. C. Fabris, and M. E. Rodrigues, Black-bounce solutions in a k-essence theory under the effects of bumblebee gravity, *Phys. Rev. D* **111**, 124005 (2025), arXiv:2503.09920 [gr-qc].

[42] C. F. S. Pereira, D. C. Rodrigues, M. V. d. S. Silva, J. C. Fabris, M. E. Rodrigues, and H. Belich, Magnetically charged black-bounce solution via nonlinear electrodynamics in a k-essence theory, *Phys. Rev. D* **111**, 084025 (2025), arXiv:2409.09182 [gr-qc].

[43] C. F. S. Pereira, D. C. Rodrigues, É. L. Martins, J. C. Fabris, and M. E. Rodrigues, New sources of ghost fields in k-essence theories for black-bounce solutions, *Class. Quant. Grav.* **42**, 015001 (2025), arXiv:2405.07455 [gr-qc].

[44] C. F. S. Pereira, D. C. Rodrigues, J. C. Fabris, and M. E. Rodrigues, Black-bounce solution in k-essence theories, *Phys. Rev. D* **109**, 044011 (2024), arXiv:2309.10963 [gr-qc].

[45] A. Lima, G. Alencar, and D. Sáez-Chillón Gómez, Regularizing rotating black strings with a new black-bounce solution, *Phys. Rev. D* **109**, 064038 (2024), arXiv:2307.07404 [gr-qc].

[46] A. C. L. Santos, L. A. Lessa, R. V. Maluf, and G. J. Olmo, Echoes and quasinormal modes of asymmetric black bounces, (2025), arXiv:2508.11096 [gr-qc].

[47] A. R. P. Moreira, A. Bouzenada, S.-H. Dong, G.-H. Sun, and F. Ahmed, Thermal Behavior of Generalized Black-Bounce Black Hole Model, (2025), arXiv:2507.20195 [gr-qc].

[48] T. M. Crispim, M. V. d. S. Silva, G. Alencar, and D. Sáez-Chillón Gómez, Tidal Stretching and Compression in Black Bounce Backgrounds, (2025), arXiv:2507.00311 [gr-qc].

[49] H. C. D. Lima Junior, R. B. Magalhães, G. J. Olmo, and D. Rubiera-Garcia, Resolving space-time singularities in spherically symmetric black holes: geodesic completeness, curvature scalars, and tidal forces, (2025), arXiv:2506.17918 [gr-qc].

[50] A. Bragado and G. J. Olmo, Periodic equatorial orbits in a black bounce scenario, (2025), arXiv:2506.15600 [gr-qc].

[51] A. Duran-Cabacés, D. Rubiera-Garcia, and D. Sáez-Chillón Gómez, Quasinormal modes and echoes of generalized black hole bounces and their correspondence with shadows, *Phys. Rev. D* **112**, 044016 (2025), arXiv:2506.10814 [gr-qc].

[52] C. F. S. Pereira, A. R. Soares, M. V. d. S. Silva, R. L. L. Vitória, and H. Belich, Light deflection and gravitational lensing effects in acoustic black-bounce spacetime, (2025), arXiv:2505.12577 [gr-qc].

[53] J. Mazza, E. Franzin, and S. Liberati, A novel family of rotating black hole mimickers, *JCAP* **04**, 082, arXiv:2102.01105 [gr-qc].

[54] Z. Xu and M. Tang, Rotating spacetime: black-bounces and quantum deformed black hole, *Eur. Phys. J. C* **81**, 863 (2021), arXiv:2109.13813 [gr-qc].

[55] Y. Yang, D. Liu, A. Övgün, Z.-W. Long, and Z. Xu, Quasinormal modes of Kerr-like black bounce spacetime, (2022), arXiv:2205.07530 [gr-qc].

[56] E. Franzin, S. Liberati, J. Mazza, R. Dey, and S. Chakraborty, Scalar perturbations around rotating regular black holes and wormholes: Quasinormal modes, ergoregion instability, and superradiance, *Phys. Rev. D* **105**, 124051 (2022), arXiv:2201.01650 [gr-qc].

[57] D. P. Viththani, T. Bhanja, V. Patel, and P. S. Joshi, Magnetic Penrose process and Kerr black hole mimickers, *Phys. Rev. D* **110**, 123035 (2024), arXiv:2407.19738 [gr-qc].

[58] F. S. Khoo, Scalar quasinormal modes of rotating regular black holes, *Phys. Rev. D* **111**, 124025 (2025), arXiv:2503.09390 [gr-qc].

[59] A. Saha, Testing Multipole Moments of compact objects beyond Kerr paradigm, (2025), arXiv:2503.00439 [gr-qc].

[60] F. L. Carneiro, S. C. Ulhoa, J. F. da Rocha-Neto, and J. W. Maluf, Irreducible mass of a regular rotating black hole, *Phys. Rev. D* **109**, 084079 (2024), arXiv:2405.05475 [gr-qc].

[61] D. Pedrotti and S. Vagnozzi, Quasinormal modes-shadow correspondence for rotating regular black holes, *Phys. Rev. D* **110**, 084075 (2024), arXiv:2404.07589 [gr-qc].

[62] Y. Yang, D. Liu, A. Övgün, G. Lambiase, and Z.-W. Long, Rotating black hole mimicker surrounded by the string cloud, *Phys. Rev. D* **109**, 024002 (2024), arXiv:2307.09344 [gr-qc].

[63] E. Franzin, S. Liberati, J. Mazza, and V. Vellucci, Stable rotating regular black holes, *Phys. Rev. D* **106**, 104060 (2022), arXiv:2207.08864 [gr-qc].

[64] A. Kamenshchik and P. Petriakova, Newman-Janis algorithm's application to regular black hole models, *Phys. Rev. D* **107**, 124020 (2023), arXiv:2305.04697 [gr-qc].

[65] Y. B. Zel'Dovich, Generation of Waves by a Rotating Body, *Soviet Journal of Experimental and Theoretical Physics Letters* **14**, 180 (1971).

[66] Y. B. Zel'Dovich, Amplification of Cylindrical Electromagnetic Waves Reflected from a Rotating Body, *Soviet Journal of Experimental and Theoretical Physics* **35**, 1085 (1972).

[67] R. Brito, V. Cardoso, and P. Pani, Superradiance, *Lect. Notes Phys.* **906**, (2015), arXiv:1501.06570 [gr-qc].

[68] S. R. Dolan, Instability of the massive Klein-Gordon field on the Kerr spacetime, *Phys. Rev. D* **76**, 084001 (2007), arXiv:0705.2880 [gr-qc].

[69] S. R. Dolan, Superradiant instabilities of rotating black holes in the time domain, *Phys. Rev. D* **87**, 124026 (2013), arXiv:1212.1477 [gr-qc].

[70] H. R. Beyer, On the stability of the massive scalar field in kerr space-time, *Journal of Mathematical Physics* **52**, 102502 (2011).

[71] H. Furuhashi and Y. Nambu, Instability of massive scalar fields in Kerr-Newman space-time, *Prog. Theor. Phys.* **112**, 983 (2004), arXiv:gr-qc/0402037.

[72] R. Brito, V. Cardoso, and P. Pani, Superradiance, *Lecture Notes in Physics* 10.1007/978-3-030-46622-0 (2020).

[73] P. H. C. Siqueira and M. Richartz, Quasinormal modes, quasibound states, scalar clouds, and superradiant instabilities of a Kerr-like black hole, *Phys. Rev. D* **106**, 024046 (2022), arXiv:2205.00556 [gr-qc].

[74] V. Cardoso and S. Yoshida, Superradiant instabilities of rotating black branes and strings, *JHEP* **07**, 009, arXiv:hep-th/0502206.

[75] S. Hod, Stationary Scalar Clouds Around Rotating Black Holes, *Phys. Rev. D* **86**, 104026 (2012), [Erratum: *Phys. Rev. D* 86, 129902 (2012)], arXiv:1211.3202 [gr-qc].

[76] W. H. Press and S. A. Teukolsky, Floating Orbits, Superradiant Scattering and the Black-hole Bomb, *Nature* **238**, 211 (1972).

[77] R. Brito, V. Cardoso, and P. Pani, Black holes as particle detectors: evolution of superradiant instabilities, *Class. Quant. Grav.* **32**, 134001 (2015), arXiv:1411.0686 [gr-qc].

[78] H. Motohashi, Resonant Excitation of Quasinormal Modes of Black Holes, *Phys. Rev. Lett.* **134**, 141401 (2025), arXiv:2407.15191 [gr-qc].

[79] J. P. Cavalcante, M. Richartz, and B. C. da Cunha, Exceptional Point and Hysteresis in Perturbations of Kerr Black Holes, *Phys. Rev. Lett.* **133**, 261401 (2024), arXiv:2407.20850 [gr-qc].

[80] J. P. Cavalcante, M. Richartz, and B. C. da Cunha, Massive scalar perturbations in Kerr black holes: Near extremal analysis, *Phys. Rev. D* **110**, 124064 (2024), arXiv:2408.13964 [gr-qc].

[81] Y. Yang, E. Berti, and N. Franchini, Black Hole Quasinormal Mode Resonances, *Phys. Rev. Lett.* **135**, 201401 (2025), arXiv:2504.06072 [gr-qc].

[82] R. K. L. Lo, L. Sabani, and V. Cardoso, Quasinormal modes and excitation factors of Kerr black holes, *Phys. Rev. D* **111**, 124002 (2025), arXiv:2504.00084 [gr-qc].

[83] J. P. Cavalcante, M. Richartz, and B. C. da Cunha, Ergodic Hysteresis of the Kerr black hole spectrum, (2025), arXiv:2511.16640 [gr-qc].

[84] P. H. C. Siqueira and M. Richartz, Data for: “superradiant scattering by rotating black-bounce black holes”, 10.5281/zenodo.17983195 (2025).